Dynamic Control of Grid-connected Microgrids for Tie-line Smoothing

Mojaharul Islam , School of Engineering & Built Environment, Griffith University, Australia
Fuwen Yang †, School of Engineering & Built Environment, Griffith University, Australia
Mohammad Amin, Department of Electric Power Engineering at Norwegian University of Science and Technology (NTNU), Norway

Abstract

This paper presents an interlink-inverter control method for providing a constant tie-line smoothing service in a grid-connected residential microgrid (MG) to mitigate the fluctuating nature of renewable generations and load demand. A grid power controller is designed for an MG to keep a constant grid power on typical days of the year by maintaining the charging/discharging of the battery. To achieve the objective, the MG controller sends the reference to the interlink-inverter controller based on the load dynamics, average PV generation & battery capacity. Moreover, a state-space model is developed from the dynamic model of the MG system and eigen value based stability analysis is done for different system parameters. The proposed control method is verified with extensive case studies by using real irradiance and typical residential customer load data in Queensland, Australia. Additionally, a comparison with a dynamic energy management based method aiming to achieve the same objective is illustrated to show the performance of the proposed control method. The results show that the proposed method gives a constant tie-line power for a grid-connected residential MG for typical days of the year.

Index Terms

Tie-line smoothing, Dynamic control, Residential microgrid, Current controller, Grid smoothing.

I. Introduction

In the last decades, the integration of renewable energy resources (RESs) in distribution networks promotes microgrids as an attractive and feasible solution to reduce the use of fossil fuels in power generation [1]. A microgrid (MG) combines distributed generations (DGs) and energy storage system (ESS) to form a small grid that feeds different loads on a low/ medium voltage network. An MG can operate in either grid-connected or island mode. Due to the economic benefits, an MG has become an attractive solution to customers in recent years. Lots of attention has been given to island MG control [2]–[6] that focuses on voltage and frequency variation in an island MG. However, the tie-line fluctuation is one of the key bottlenecks in a grid-connected MG due to the variation of power from RESs and load demand. Tie-line fluctuation in grid-connected MGs can cause severe stability and quality issues for the distribution network. Previous research addresses this problem by controlling the power of MG resources like non-renewable generation control, demand side control, ESS control or coordinate control through an energy management system (EMS) of the MG [7]–[16].

Demand side control is one of the control approaches to mitigate tie-line fluctuations through direct or indirect (load scheduling, power pricing) control of load demand [7], [8]. A demand side control is presented in [7] by directly and continuously modulating load power consumption in an industrial MG. In [9], a large number of controllable loads are described as virtual energy storage in parallel with battery storage and a fuzzy logic controller is applied to revise the range of the virtual energy storage. Coordinated control between a heat pump and battery storage is proposed in [10] to smooth the tie-line power fluctuations in a group of residential MGs. Similarly, a hybrid electro-thermal storage is formed in [11] using a battery and a hot water tank to optimize the power exchange with the grid in an electro-thermal residential MG. In [8], [12], a peak power pricing mechanism is used along with short-term forecasting of renewable generations to smooth the power exchange with the grid. In those studies, a mixed-integer linear programming problem is integrated into a model predictive control framework to reduce the forecasting error. Besides that, tie-line smoothing can be achieved through coordinated control among controllable loads, the battery and non-renewable generation. A scheduling method among a diesel generator, battery storage and different controllable loads is performed in [13] through an EMS of an MG to reduce the tie-line fluctuations. Coordinate control is also possible between the diesel generator and battery storage where demand side control is not allowed. In [14], a power management system is proposed to share the local load with the main grid by controlling the diesel generator using droop reference estimator and the battery using a current controller. However, demand side control is not possible for most of the real residential MG due to service reliability. Moreover, most of the residential MG do not have a diesel generator and mostly depends on RESs as a primary resource inside the MG. Therefore, the tie-line smoothing objective is more challenging for a grid-connected residential MG where battery storage is the only controllable unit, and reliability of the customer is more

† Corresponding author: Fuwen Yang, School of Engineering & Built Environment, Griffith University, Parkland Dr, Southport, QLD-4215, Australia. e-mail:fuwen.yang@griffith.edu.au

important than demand side control. Thus the above methods may not be applicable to obtain a smooth tie-line service in a residential MG.

Previous research have applied different control methods to deal with the tie-line fluctuation problem of a residential MG based on forecasting or historical weather information. Considering the prediction of the MG future power, a mixed-integer linear program is used in [17] to reduce the tie-line power fluctuation along with minimizing the operation cost of the battery and energy usage.A fuzzy logic based supervisory control is implemented in [18] to minimize forecasted utility power reference by adjusting the set points of DGs. Forecasting method is also used in [19], [20] to smooth the tie-line power in a residential MG operation. A centralized moving average strategy [19] and a fuzzy logic-based control [20] has been proposed in an EMS of MG to reduce the forecasting error by maintaining the battery state of charge (SoC). Besides that, in [21], a fuzzy logic based tie-line smoothing controller is designed for a residential MG without any forecasting by taking the energy rate-of-change and the battery state of charge as inputs to modify the required adjustment of grid power. After the adjustment of grid power, the necessary control of the battery is determined using the power balance equation of the MG. Moreover, a hierarchical power scheduling control strategy is proposed in [22] to ensure a flat grid power in a multi-microgrid network consisting, of a large number of DERs. All of the previous study contemplates a specific duration such as 10 minutes to an hour to schedule the tie-line power. Thus, those methods are difficult to apply to resolve the short-term fluctuation problems i.e. 5 minutes or less, caused by the RESs and load.

A short-term tie-line fluctuation is analyzed in [23], and a fuzzy logic controller is designed in a dynamic EMS to control the battery in a grid-connected residential MG. However, the result shows that the method is reduced tie-line fluctuation but unable to maintain constant tie-line control. Moreover, the afore-mentioned previous work did not mention the detailed control architecture nor any dynamic model of the MG. Consequently, it is difficult to design any dynamic controller for mitigating the dynamic behavior of renewable generation or loads. As far the authors know, the tie-line fluctuation problem in a grid-connected residential MG is not addressed in the previous study using the dynamic analysis of the system. Therefore, designing a dynamic controller is appealing to resolve this issue. This paper proposes a grid power control method for the interlink-inverter of the MG to maintain a constant tie-line power for typical days of the year. The controller combined with an outer loop droop based power controller and inner loop grid current controller. The reference grid power is given by the MG controller and determined in the design stage based on the load dynamics, PV generation and battery capacity. The reference current of the grid current controller is calculated by using reference grid power from the droop controller and grid voltage. The proposed constant power control method is also able to obtain other tie-line objectives like power smoothing, flat tie-line power, peak shaving and power ramp limitation. In the MG, the battery module connects with the PV converter in a hybrid configuration to reduce the number of conversions. The DC/DC converter in the battery module is responsible for maintaining the DC link voltage of the MG through the charging/ discharging operation of the battery in coordination with the proposed current controller. Furthermore, a dynamic model of the MG is developed from the time average model of a typical grid-connected residential MG. A close loop state-space model of the MG system is derived from the dynamic model of the MG and eigen value based stability analysis is done for different system parameters. The proposed controller is verified with extensive case studies by using real irradiance and typical residential customer load data in Queensland, Australia. The results show that the proposed controller is maintaining a constant tie-line power set by the MG controller by secure charging/discharging of the battery. Moreover, a comparison with a dynamic EMS based method to obtain the same goal is presented in MATLAB simulation. The main contribution of this article in state of the art:

(1) A constant grid power control method is proposed for the interlink inverter of a grid-connected residential MG to obtain a smooth tie-line service despite the variation of RESs and load demand.

(2) A state-space model is derived from the dynamic model of the MG to analysis the dynamic response of the controller in different case studies.

(3) A comparison with the dynamic EMS method is presented to illustrate the performance of the proposed control method.

The rest of the paper is organized as follows: Section 2 describes the system configuration and control strategies, Section 3 illustrates Modeling and stability analysis of the MG, Section 4 presents simulation results and comparisons for different case studies, and Section 5 concludes the article.

II. System Configuration & Control Strategies

The study considers a typical grid connected residential AC MG structure with a PV panel as RES, a battery as an ESS and a residential load. The PV panel and battery are connected to the grid in hybrid configuration. A rated capacity of 2.5 KW solar panel and a battery of 17KWh are installed for supply in a typical single residential house of Queensland, Australia with an average demand of 15KWh per day. Fig.1 depicts the MG test setup in Griffith for the system under study. Besides that, the system assumes a robust communication structure between different units of the study MG. The system has three converters to fulfill the control requirements. The boost converter in PV unit is used to track the maximum power from the PV panel. The buck-boost converter is connected the battery storage system with the DC link. The converter is designed to maintain the DC link voltage to the reference through charging/discharging of the battery. The DC link is connected to AC bus through an interlink inverter. The interlink inverter control is designed to control the grid power drawn by the MG. In this

paper, a constant grid power control method is proposed to maintain a constant tie-line power for typical days of the year. The detailed control strategies are illustrated in the following subsections.

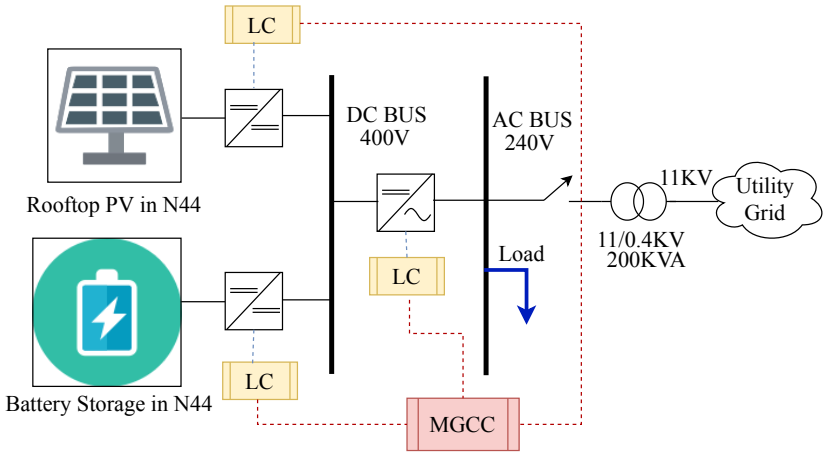

Fig. 1. A typical grid-connected residential AC MG setup in Building N44,Griffith University

A. MMPT Control

The boost converter connected with the PV panel is considered as an ideal MPPT controller using perturb & observe (P & O) method to track the maximum power from the PV unit [24].

B. DC Link Voltage Control

The bidirectional buck-boost converter connected with the battery storage is responsible for maintaining the DC link voltage. The idea of using charge/discharge power of the battery banks to regulate the DC voltage (by means of a PI controller) has been introduced in [5], [25]. If the measured DC link voltage is greater than the reference voltage, the battery will run in buck mode to charge the battery. If the measured DC link voltage is smaller than the reference voltage, the battery will run in boost mode to discharge the battery. Otherwise, the battery will be in rest mode without any buck-boost operation. However, to limit over charging/discharging of battery, an SoC based EMS is applied in the system that will discuss in the following section (3.3). The Fig.2 shows the flowchart to decide on buck or boost operation of the converter and Fig.3 shows the block diagram of the DC link voltage controller. The equations of the controller are illustrated in equations (1-2).

where

$$d_2 = K_{p1}(v_{dc}^* - v_{dc}) + K_{i1}\gamma \tag{1}$$

$$\gamma = \int (v_{dc}^* - v_{dc}) \tag{2}$$

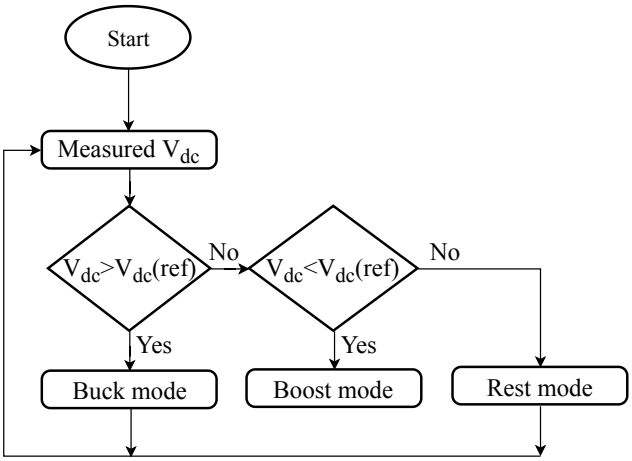

Fig. 2. Flow chart of DC link voltage controller to regulate battery charging/discharging

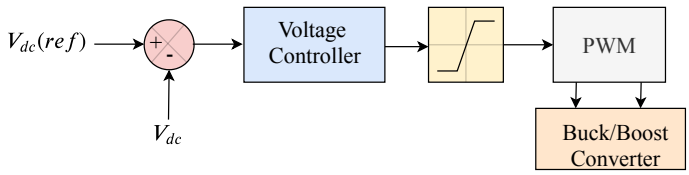

Fig. 3. DC link voltage controller

C. Proposed Grid Power Control

A DC/AC bidirectional inverter control method is proposed to control the grid power draw by the MG and to obtain a constant tie-line of a grid-connected MG despite the fluctuating nature of RESs and load demand. The proposed method is followed three steps hierarchical control approach to control the grid power. In the first step, a process to determine the grid power reference is described to obtain a constant tie-line for typical days of the year. The day to day variation of the renewable generation and load demand will vary the average daily power drawn by the MG. The commercial software like HomerPro usually use the statistical data of power generations and demand to calculate the average power shortage of the MG throughout the year. The shortage power needs to supply by the utility grid to balance the power inside the MG. Based on the system configuration and statistical data of the MG, the algorithm determines the percentage of the average load needs to be supplied by the utility grid for typical days of the year. The result may vary based on the available generation capacity, generation type, load dynamics and geographical location of the MG. After that, the reference grid power is feed to the MG controller to provide the control reference to the interlink inverter of the MG. Generally, an MG controller is responsible for performing different types of activities like power flow control, secondary voltage and frequency regulation, economic operation etc based on the control requirements of an MG. However, this paper only focuses on power flow control of the MG to obtain a constant tie-line power in a grid-connected residential MG. A battery SoC based EMS is applied to control the grid power and to limit the over charging/discharging of the battery. When the battery SoC is within the predefined limit, the MG controller provided a constant reference power determined by the algorithm. If the battery SoC is over SoC_{max} due to over-generation from PV panel, the reference grid power is set equal to $P_{pv} - P_{load}$ to transfer the excess generation to the grid. On the other side, if the battery SoC is under SoC_{min}, the MG controller sets the grid reference power to maintain a reliable power supply to the load demand in the MG. In both cases, the grid reference power is set to a value so that the battery will not over charge/discharge to keep a healthy life of the battery storage system. Fig.4 shows the process to determine the reference gird power to supply to the interlink inverter.

In the second step, a combination of droop control and current calculation method is introduced to determine the reference grid current from the reference grid power set by the MG controller. A droop control method is used to control the real and reactive power reference according to the grid frequency and voltage. The droop control feature will also enable the interlink inverter for coordinate operation with other inverters in a multi-microgrid based distribution network. This paper adopts the conventional droop control method between P-ω and Q-V is illustrated in equation 3.

$$\begin{aligned} \omega &= \omega^* - m(P - P^*) \\ V &= V^* - n(Q - Q^*) \end{aligned} \tag{3}$$

The droop co-efficient can be calculated using the following equation,

$$\begin{aligned} m &= \frac{2\pi(f_{max} - f_{min})}{P_{max}} \\ n &= \frac{(V_{max} - V_{min})}{Q_{max}} \end{aligned} \tag{4}$$

As the reactive power reference of the inverter usually set to $Q^* = 0$ in grid-connected operation, only P-ω droop is implemented in this paper. f_{max},f_{min} are chosen according to the Australian power system standard and P_{max} is the rated power of the inverter. The power determined by the droop controller is used to calculate the reference current of the grid current controller.

The real and reactive power equations for a single phase system in d-q reference frame can be written as,

$$\begin{aligned} P_g &= \frac{1}{2}(v_{gd}i_{gd} + v_{gq}i_{gq}) \\ Q_g &= \frac{1}{2}(v_{gq}i_{gd} + v_{gd}i_{gq}) \end{aligned} \tag{5}$$

The equation 5 is used to calculate the reference current of the inverter is illustrated in equation 6.

$$i_{gd}^{*} = \frac{2P_g^{*} v_{ogd} + 2Q_g^{*} v_{ogq}}{v_{ogd}(v_{ogd}^2 + v_{ogq}^2)}$$
$$i_{gq}^{*} = \frac{2P_g^{*} v_{ogd} v_{ogq} - 2Q_g^{*} v_{ogd}^2}{(v_{ogd}^2 + v_{ogq}^2)} \tag{6}$$

In the third step, a grid current controller is designed to control the interlink inverter of a grid-connected MG to track the grid current to the reference determined by the second step of the control method. Fig.5 shows the block diagram of the designed grid current controller with a detail control structure to determine the duty cycle of the inverter. The equations of the grid current controller are illustrated in equations (7-10).

$$v_{id} = v_{od} - \omega L_f i_{fq} + R_f i_{fd} + K_{p2}(i_{gd}^{*} - i_{gd}) + K_{i2}\beta_{id} \tag{7}$$
$$\beta_{id} = \int (i_{gd}^{*} - i_{gd}) \tag{8}$$
$$v_{iq} = v_{oq} + \omega L_f i_{fd} + R_f i_{fq} + K_{p2}(i_{gq}^{*} - i_{gq}) + K_{i2}\beta_{iq} \tag{9}$$
$$\beta_{iq} = \int (i_{gq}^{*} - i_{gq}) \tag{10}$$

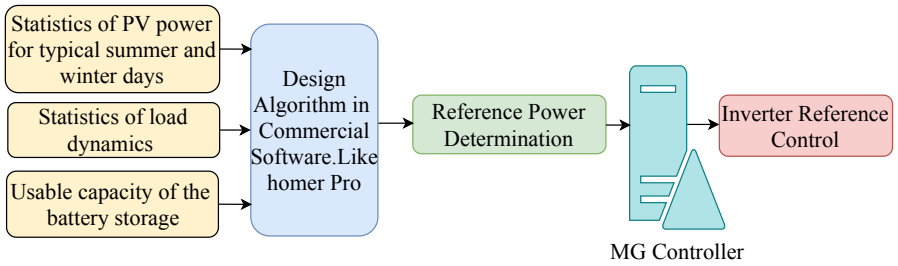

Fig. 4. Process to determine the reference power of the interlink inverter

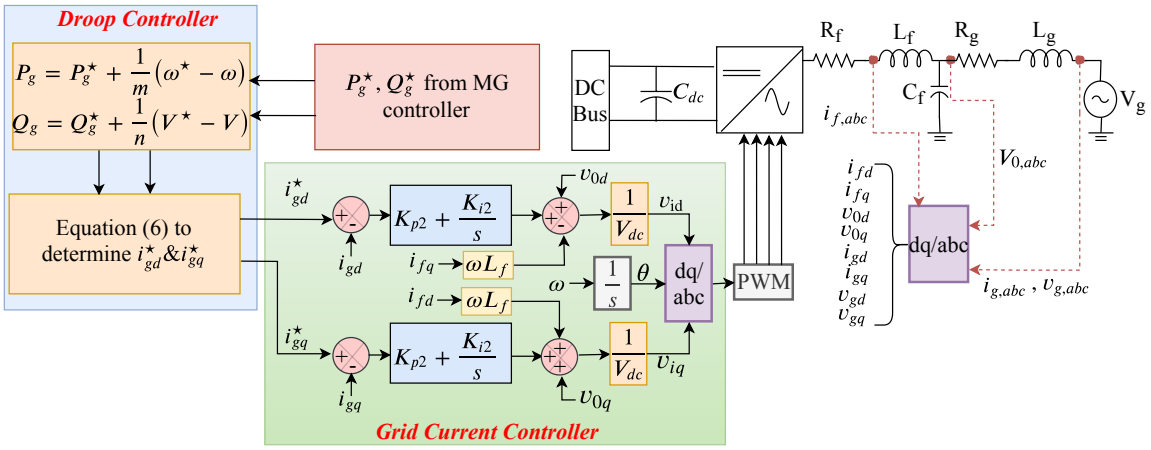

Fig. 5. Proposed grid power controller

III. Modeling and Stability Analysis of Microgrid

A. Modeling of Microgrid

According to Fig.1, the PV panel is connected to the DC link through a DC-DC boost converter. The battery module is connected to the DC link through a bidirectional buck-boost converter. The DC link of the MG is connected to the point of common coupling (PCC) through a bidirectional DC-AC inverter and an LC filter. In addition, the MG load is considered as a residential load connected at PCC. However, the MG model in the figure can be represented by the differential equations to derive the analytical model of the MG.

The voltage and current equations of DC-DC converters and the DC link are illustrated as,

$$L_1 \frac{di_1}{dt} = v_{pv} - R_1 i_1 - (1 - d_1) v_{dc} \tag{11}$$

$$L_2\frac{di_2}{dt} = v_{bat} - R_2 i_2 - (1-d_2)v_{dc} \tag{12}$$

$$C_{dc}\frac{dv_{dc}}{dt} = (1-d_1)i_1 - (1-d_2)i_2 - d_d i_d - d_q i_q \tag{13}$$

Similarly, the ac side voltage and current equations with inverter can be written in d-q reference frame as,
Inverter loop equations,

$$L_f\frac{di_{fd}}{dt} = v_{id} - R_f i_{fd} + \omega L_f i_{fq} - v_{od} \tag{14}$$

$$L_f\frac{di_{fq}}{dt} = v_{iq} - R_f i_{fq} - \omega L_f i_{fq} - v_{oq} \tag{15}$$

Grid loop Equations,

$$L_g\frac{di_{gd}}{dt} = -R_g i_{gd} + \omega L_g i_{gq} + v_{od} - v_{gd} \tag{16}$$

$$L_g\frac{di_{gq}}{dt} = -R_g i_{gq} - \omega L_g i_{gd} + v_{oq} - v_{gq} \tag{17}$$

Equations of filter capacitor,

$$C_f\frac{v_{od}}{dt} = i_{fd} - i_{gd} - i_{Ld} + \omega C_f v_{oq} \tag{18}$$

$$C_f\frac{v_{oq}}{dt} = i_{fq} - i_{gq} - i_{Lq} - \omega C_f v_{od} \tag{19}$$

B. Phase Locked Loop(PLL) Control

The PLL is necessary to track the actual frequency of the system. The input of the PLL is the d-axis component of the voltage across the filter capacitor. Thus the phase is locked at $v_{od} = 0$ [26]. The equations (23-25) illustrate the states associated with PLL.

$$\frac{dv_{odf}}{dt} = \omega_{cPLL} v_{od} - \omega_{cPLL} v_{odf} \tag{20}$$

$$\frac{d\phi_{PLL}}{dt} = -v_{odf} \tag{21}$$

$$\frac{d\theta}{dt} = \omega_g - k_{pPLL} v_{odf} + k_{iPLL}\phi_{PLL} \tag{22}$$

C. Small Signal Model

To derive the small-signal model of the MG and to simplify the analysis, the boost converter and the PV panel are replaced by an ideal variable current source. Accordingly, the DC link voltage equation can be simplified as,

$$C_{dc}\frac{dv_{dc}}{dt} = i_1 - (1-d_2)i_2 - d_d i_d - d_q i_q \tag{23}$$

The differential equations in (1-2), (7-8) & (12-22) are used to derive the closed-loop nonlinear system model of the study MG. The nonlinear system model needs to be linearized near a steady state point for stability analysis of the system. The steady state operating point of the system can be derived by solving this nonlinear system model with derivatives terms set to zero. The linearized small signal model of the MG is represented using the standard state-space equations as,

$$\begin{aligned} \Delta\dot{x} &= A\Delta x + B\Delta u \\ y &= C\begin{bmatrix}\Delta i_{gd} \\ \Delta i_{gq}\end{bmatrix} + D\Delta u \end{aligned} \tag{24}$$

where the state variables Δx and system inputs Δu are represented in equations (25-26) and the system coefficients are illustrated in equations (27-35).

$$\Delta x = [\Delta i_2 \quad \Delta v_{dc} \quad \Delta\gamma \quad \Delta i_{fd} \quad \Delta i_{fq} \quad \Delta\beta_{id} \quad \Delta\beta_{iq} \quad \Delta i_{gd} \quad \Delta i_{gq} \quad \Delta v_{od} \quad \Delta v_{oq} \quad \Delta v_{odf} \quad \phi_{PLL} \quad \theta] \tag{25}$$

$$\Delta u = \begin{bmatrix}\Delta i_1 & \Delta v^*_{dc} & \Delta v_{bat} & \Delta i^*_{gd} & \Delta i^*_{gq} & \Delta v_{gd} & \Delta v_{gq} & \Delta i_{Ld} & \Delta i_{Lq}\end{bmatrix} \tag{26}$$

$$A = \begin{bmatrix} -\frac{R_2}{L_2} & A_{12} & \frac{(K_{i1}V_{dc})}{L_2} & 0 & 0 & 0 & 0 & 0 & 0 & 0 & 0 & 0 & 0 & 0 \\ A_{21} & A_{22} & \frac{-(K_{i1}I_2)}{C_{dc}} & A_{24} & A_{25} & \frac{-(K_{i2}I_{fd})}{(C_{dc}V_{dc})} & \frac{-(K_{i2}I_{fq})}{(C_{dc}V_{dc})} & \frac{(K_{p2}I_{fd})}{(C_{dc}V_{dc})} & \frac{(K_{p2}I_{fq})}{(C_{dc}V_{dc})} & \frac{-I_{fd}}{(C_{dc}V_{dc})} & \frac{-I_{fq}}{(C_{dc}V_{dc})} & 0 & 0 & 0 \\ 0 & -1 & 0 & 0 & 0 & 0 & 0 & 0 & 0 & 0 & 0 & 0 & 0 & 0 \\ 0 & 0 & 0 & 0 & 0 & \frac{K_{i2}}{L_f} & 0 & \frac{-K_{p2}}{L_f} & 0 & 0 & 0 & 0 & 0 & 0 \\ 0 & 0 & 0 & 0 & 0 & 0 & \frac{K_{i2}}{L_f} & 0 & \frac{-K_{p2}}{L_f} & 0 & 0 & 0 & 0 & 0 \\ 0 & 0 & 0 & 0 & 0 & 0 & 0 & -1 & 0 & 0 & 0 & 0 & 0 & 0 \\ 0 & 0 & 0 & 0 & 0 & 0 & 0 & 0 & -1 & 0 & 0 & 0 & 0 & 0 \\ 0 & 0 & 0 & 0 & 0 & 0 & 0 & 0 & \frac{-R_g}{L_g} & \omega & \frac{1}{L_g} & 0 & 0 & 0 \\ 0 & 0 & 0 & 0 & 0 & 0 & 0 & -\omega & \frac{-R_g}{L_g} & 0 & \frac{1}{L_g} & 0 & 0 & 0 \\ 0 & 0 & 0 & \frac{1}{C_f} & 0 & 0 & 0 & \frac{-1}{C_f} & 0 & 0 & \omega & 0 & 0 & 0 \\ 0 & 0 & 0 & 0 & \frac{1}{C_f} & 0 & 0 & 0 & \frac{-1}{C_f} & -\omega & 0 & 0 & 0 & 0 \\ 0 & 0 & 0 & 0 & 0 & 0 & 0 & 0 & 0 & \omega_{cPLL} & 0 & -\omega_{cPLL} & 0 & 0 \\ 0 & 0 & 0 & 0 & 0 & 0 & 0 & 0 & 0 & 0 & 0 & -1 & 0 & 0 \\ 0 & 0 & 0 & 0 & 0 & 0 & 0 & 0 & 0 & 0 & 0 & -K_{pPLL} & 0 & K_{iPLL} \end{bmatrix} \tag{27}$$

$$A_{12} = \frac{(K_{i1}\gamma + K_{p1}(V_{dc}^* - 2V_{dc}) - 1)}{L_2} \tag{28}$$

$$(A_{21} = \frac{-(K_{i1}\gamma + K_{p1}(V_{dc}^* - 2V_{dc}) - 1)}{Cdc} \tag{29}$$

$$A_{22} = \frac{(K_{p1}I_2 + \frac{(I_{fd}(V_{od}+K_{i2}\beta_{id}+R_fI_{fd}+K_{p2}(I_{gd}^*-I_{gd})-L_fI_{fq}\omega))}{V_{dc}^2} + \frac{(i_{fq}(V_{oq}+K_{i2}\beta_{iq}+R_fI_{fq}+K_{p2}(I_{gq}^*-I_{gq})+L_fI_{fd}\omega))}{V_{dc}^2}}{C_{dc}} \tag{30}$$

$$A_{24} = \frac{-(v_{od} + K_{i2}\beta_{id} + R_f * I_{fd} + K_{p2}(I_{gd}^* - I_{gd}) - L_fI_{fq}\omega + R_fI_{fd} + L_fI_{fq}\omega)}{V_{dc}C_{dc}} \tag{31}$$

$$A_{25} = \frac{-(V_{oq} + K_{i2}\beta_{iq} + R_fI_{fq} + K_{p2}(I_{gq}^* - I_{gq}) + L_fI_{fd}\omega + R_fI_{fq} - L_fI_{fd}\omega}{V_{dc}C_{dc}} \tag{32}$$

$$B = \begin{bmatrix} 0 & \frac{(K_{p1}V_{dc})}{L_2} & \frac{1}{L_2} & 0 & 0 & 0 & 0 & 0 & 0 \\ \frac{1}{C_{dc}} & \frac{-(K_{p1}I_2)}{C_{dc}} & 0 & \frac{-(K_{p2}I_{fd})}{C_{dc}V_{dc}} & \frac{-(K_{p2}I_{fq})}{C_{dc}V_{dc}} & 0 & 0 & 0 & 0 \\ 0 & 1 & 0 & 0 & 0 & 0 & 0 & 0 & 0 \\ 0 & 0 & 0 & \frac{K_{p2}}{L_f} & 0 & 0 & 0 & 0 & 0 \\ 0 & 0 & 0 & 0 & \frac{K_{p2}}{L_f} & 0 & 0 & 0 & 0 \\ 0 & 0 & 0 & 1 & 0 & 0 & 0 & 0 & 0 \\ 0 & 0 & 0 & 0 & 1 & 0 & 0 & 0 & 0 \\ 0 & 0 & 0 & 0 & 0 & \frac{-1}{L_g} & 0 & 0 & 0 \\ 0 & 0 & 0 & 0 & 0 & 0 & \frac{-1}{L_g} & 0 & 0 \\ 0 & 0 & 0 & 0 & 0 & 0 & 0 & \frac{-1}{C_f} & 0 \\ 0 & 0 & 0 & 0 & 0 & 0 & 0 & 0 & \frac{-1}{C_f} \\ 0 & 0 & 0 & 0 & 0 & 0 & 0 & 0 & 0 \\ 0 & 0 & 0 & 0 & 0 & 0 & 0 & 0 & 0 \\ 0 & 0 & 0 & 0 & 0 & 0 & 0 & 0 & 0 \end{bmatrix} \tag{33}$$

$$C = \begin{bmatrix} 0 & 0 & 0 & 0 & 0 & 0 & 0 & 1 & 0 & 0 & 0 & 0 & 0 & 0 \\ 0 & 0 & 0 & 0 & 0 & 0 & 0 & 0 & 1 & 0 & 0 & 0 & 0 & 0 \end{bmatrix} \tag{34}$$

$$D = 0 \tag{35}$$

D. Eigen Value based Stability Analysis

The linearized system model represented by the state-space equation is reflecting the accurate model of the system. The linearized system model can be used for investigating the eigen value based stability analysis of the system. The system coefficient matrix A is used to determine the states of eigenvalues in all modes of the system. The system eigenvalues for the steady state operating point based on the given conditions in Table 2 are represented in Table 1. It can be observed that the system eigenvalues in Table 1 have two poles meet in the origin and several poles close to the real axis with small damping and low oscillation frequency. There are two pairs of complex conjugate poles with high oscillation frequency related to the inverter parameters. As the system is stable for the system parameter in Table 2, a full range of investigation has done for changing the power reference from $-P_{rated}$ to P_{rated}. It is assumed that all other parameters in Table 2 are constant except the steady state value of the grid power to find the result in Fig.6. The result shows that none of the system poles is moving due to a change of steady state grid power. A similar investigation has been done for the change of PV power for the full range of operating points from 0 to $P_{pv,max}$ considering other parameters in Table 2 are constant. Fig.7 shows that the poles are almost constant despite the change of PV operating condition. A similar analysis can be done for other system parameters to find out the sensitivity of the parameters on system poles movement. However, the sensitivity of the controller gain is an important part of eigen value analysis. The sensitivity range of the controller gain has direct impact on system stability. To investigate the sensitivity of the eigen values to variations of current controller proportional gain K_{p2}, the value has increased from 0 to 2. Fig. 8 shows the trajectory of the poles with the increase of K_{p2} from 0 to 3. The result shows that poles with high imaginary part move to the right half of the axis for a controller gain more than 2. Thus, the controller gain can vary in wider range and the system will be unstable for large value of controller gain. A similar sensitivity analysis of the system eigen values has been done for the change of DC-DC converter gain. Fig.9 shows the trajectory of the poles with the increase of k_{p1} from 1 to 2.5. The result shows that the poles related to DC-DC converter gain k_{p1} has moved to the right half plane with the increase of the controller gain near 2 while other parameters of the system fixed. Further investigation of the sensitivity analysis of the eigen values can be done for other system parameters as long as few parameters are responsible for stability problem for a specific system configuration. Such investigation is a vital part of the stability analysis of the MG with different system parameters, size and number of generations in the system.

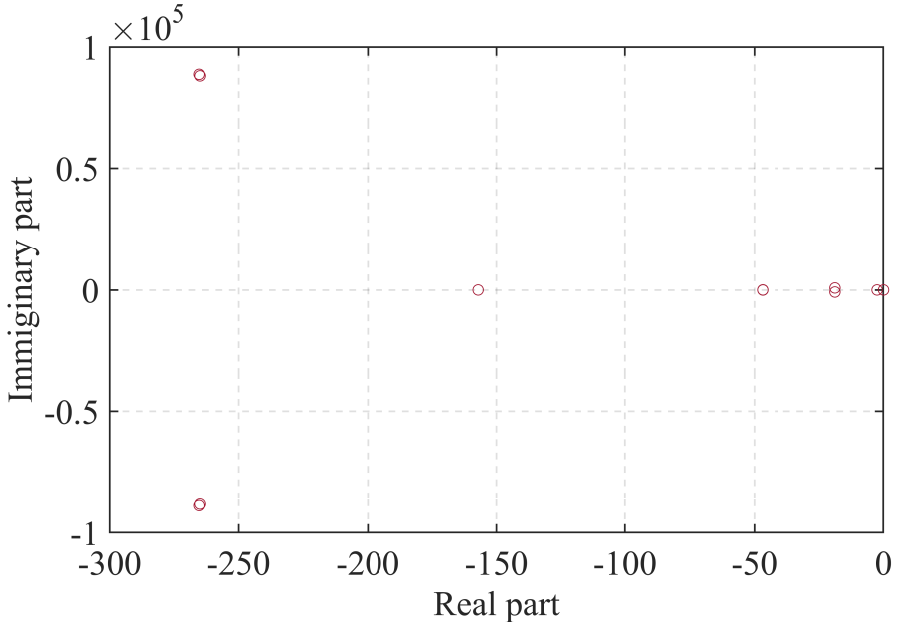

Fig. 6. Trajectory of eigen values when the power P_g^* has changed through the operating range of the inverter

IV. Simulation Results & Comparisons

A. Simulation Results

The performance of the proposed inverter control method is analyzed in the context of Queensland, Australia in simulation with real residential house load, solar radiation and temperature data. A test MG has been designed using the available resources in Griffith University, Australia. Fig.1 shows the MG setup in building N44, Griffith University. A capacity of 2.5KW peak SunPower E20 series model PV unit is used in the simulation that installed in N44. The sun radiation and temperature data of Brisbane, Australia in September 2017 are obtained from building N44, Griffith University statistical weather information database. The radiation and temperature data has been taken from 5 am to 7 pm at 1min intervals for a typical summer and

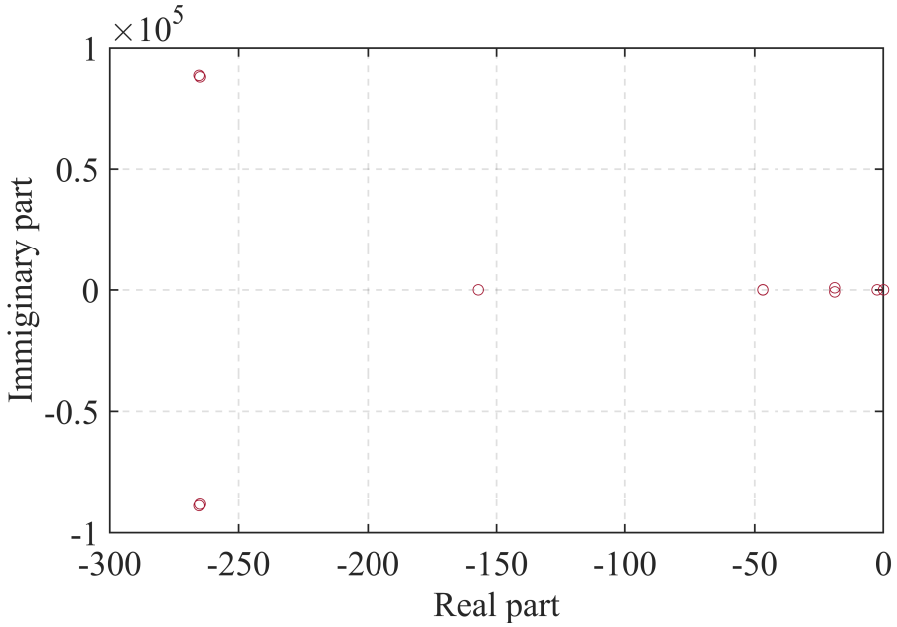

Fig. 7. Trajectory of eigen values when the power P_{pv} has changed through the operating range of the PV

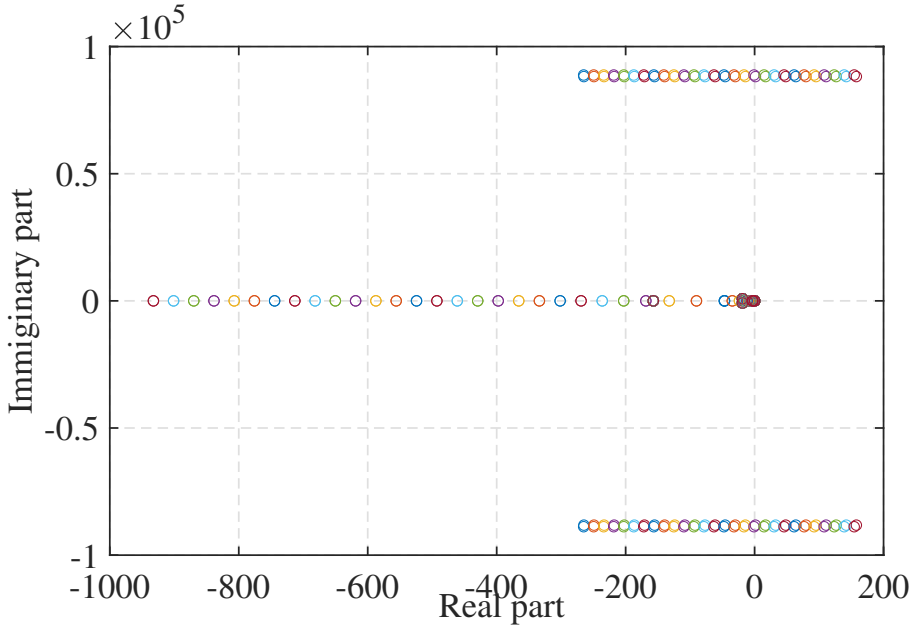

Fig. 8. Trajectory of eigen values for a change of proportional gain of the inverter

TABLE I
SYSTEM EIGEN VALUES OF THE CORRESPONDING STATES

System states	Eigen value ($\lambda_i = \sigma_i + j\omega_i$)
λ_1	0+j0
λ_2	0+j0
λ_3	-157+j0
$\lambda_{4,5}$	-265 $\pm$ j88825
$\lambda_{6,7}$	-265 $\pm$ j88197
$\lambda_{8,9}$	-19 $\pm$ j843
$\lambda_{10,11}$	-20+j0, -47+j30
λ_{12}	-47+j30
λ_{13}	-47+j30
λ_{14}	-47+j30

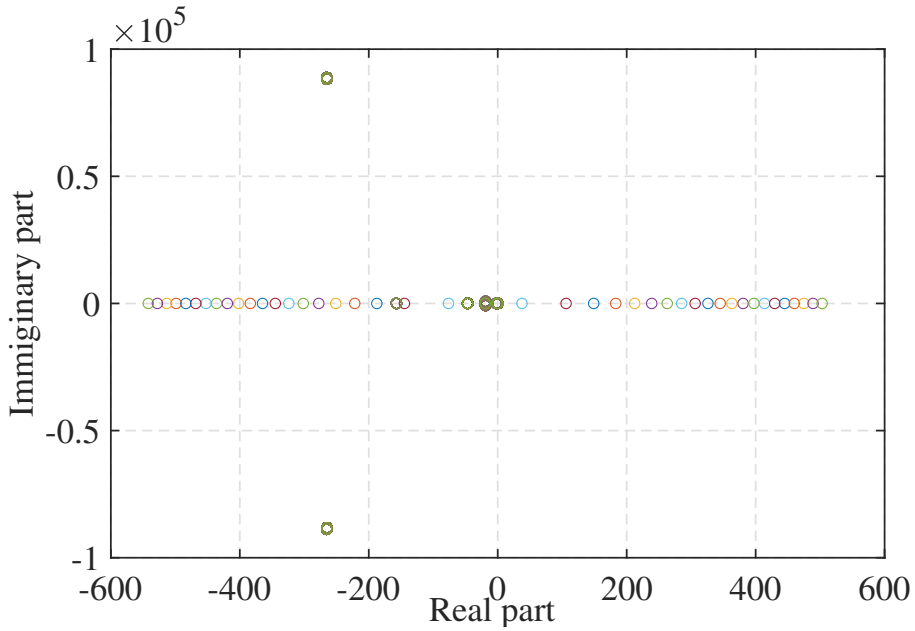

Fig. 9. Trajectory of eigen values for a change of proportional gain of the DC-DC converter

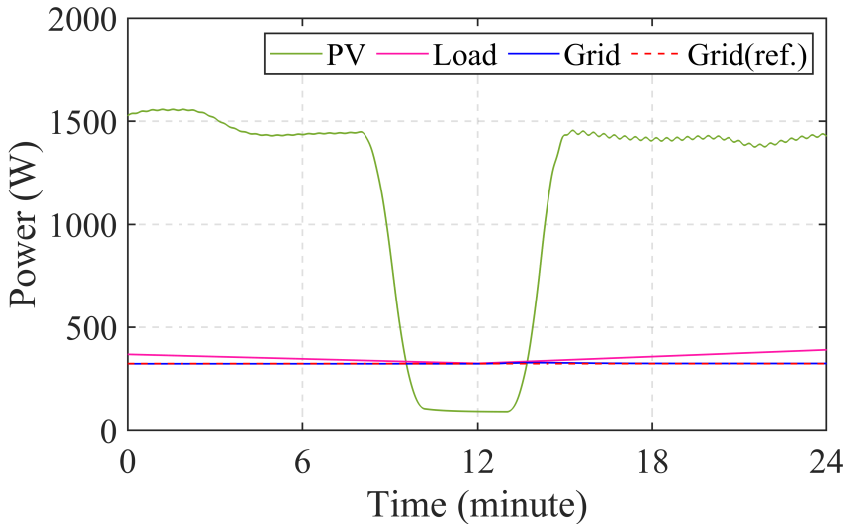

Fig. 10. Dynamic response of the controller due to sudden cloud appearance

TABLE II
SYSTEM PARAMETERS FOR STUDY MG

Symbol	Parameter	Value
L_2	Inductor value of the buck-boost converter	9mH
R_2	Resistor value of the buck-boost converter	0.25Ω
C_{dc}	Dc link capacitance	300mF
L_f	Filter inductor	3.2mH
R_f	Filter resistor	0.008Ω
C_f	Filter capacitance	9.67μF
L_g	Grid inductor	0.064 mH
R_g	Grid resistor	0.008Ω
ω_{cPLL}	PLL filter cut-off frequency	25Hz
ω	Rated frequency	50Hz
$P_(rated)$	Rated power of inverter	2.5KW
V_{rated}	Rated voltage	240 V

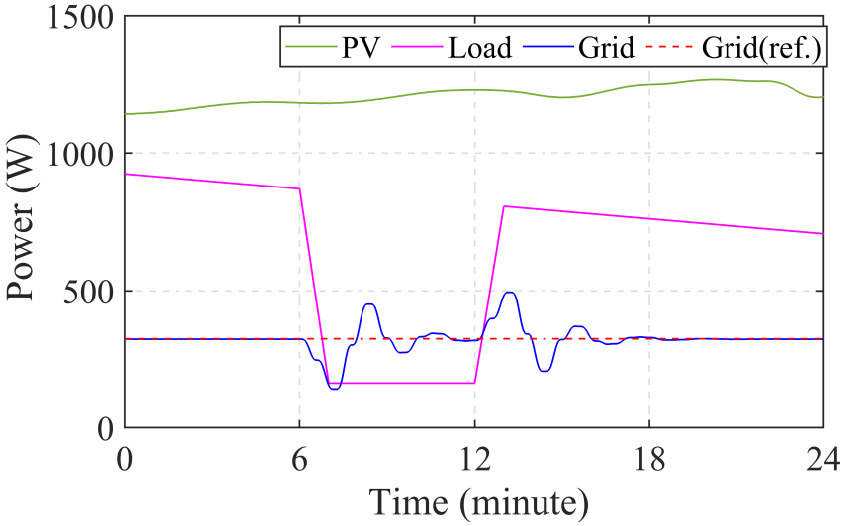

Fig. 11. Dynamic response of the controller due to short-term load variation

winter day. Furthermore, a typical residential house of Queensland load data has been collected at 1 min intervals to illustrate the load variation of the MG. Moreover, a lithium-ion battery with a rated capacity of 16KWh is installed in the system [2]. The depth of discharge (DoD) of the battery storage has been set to 90% for the residential application. Four different case studies have been done using weather and load variation to validate the dynamic performance of the controller. Considering the system dynamics, the MG controller set the reference grid power as 13% of the inverter rated power that determined in design stage of the MG. In other word, MG will draw a constant power from grid through tie-line which is 13% of the inverter rated power. Besides that, the information in table 2 is used to drive the state-space model of the study MG in MATLAB. The state-space model is used to represent the MG system model. Several case studies has done to show the performance of the controller for short-term changes of input and output system disturbances. In the study MG, the input disturbance is the variation of solar radiation and the output disturbance is load power variation. In addition, the controller performance is also shown for typical summer and winter days of the year with the variation of weather and load profile. The simulation is run for 24 hours with a time step of 1 min.

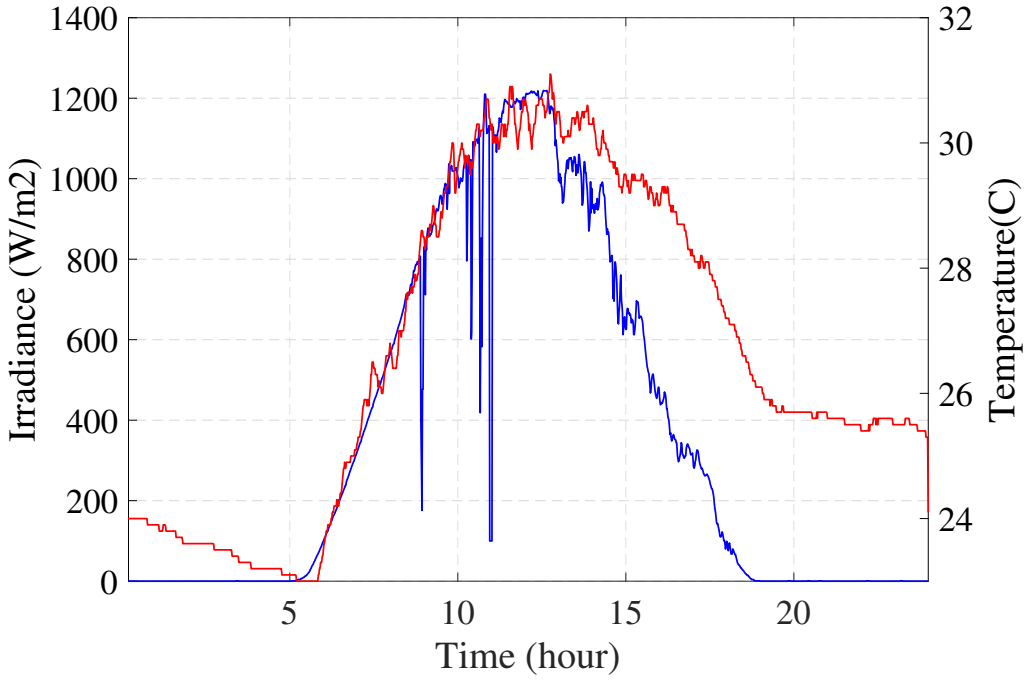

Fig. 12. Radiation and temperature for a typical summer day (25th Janunary 2017)

1) Case I: Effect of Sudden Cloudy Appearance: Weather variations has direct effect on the power generation from PV panel. To observe the effect of sudden weather variations on controller performance, this case illustrates an event of sudden

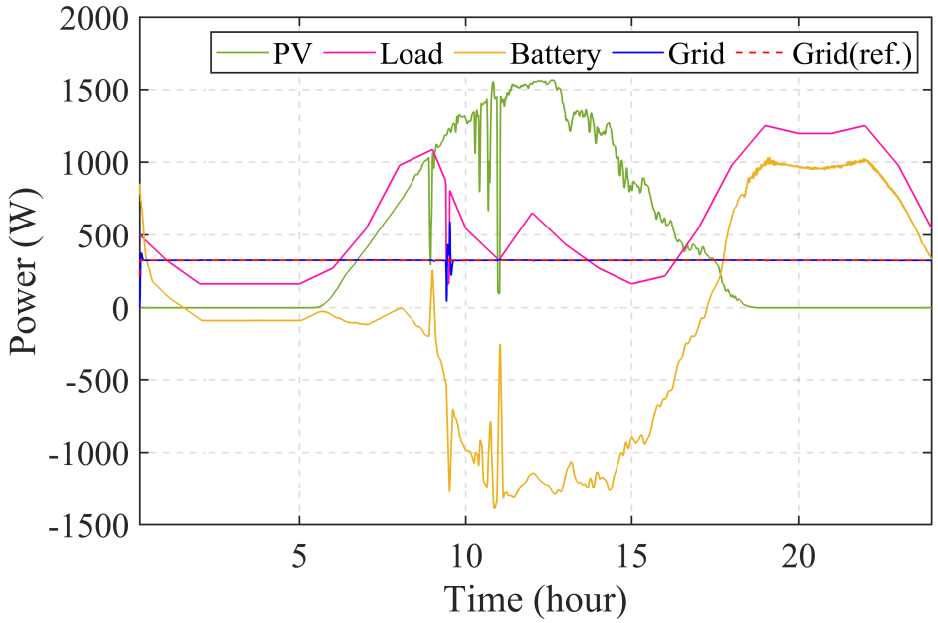

Fig. 13. PV generation, Residential load, battery power, grid power and grid power reference for a typical summer day

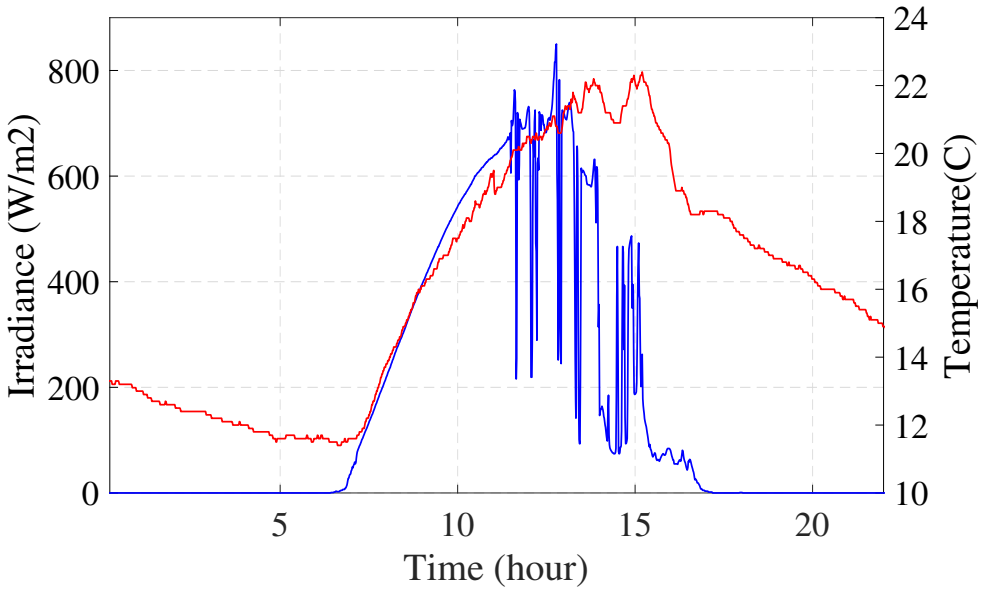

Fig. 14. Radiation and temperature for typical winter days (4th June 2017)

cloud appearance for a short period of time. During this time period, the system load is considered almost constant. To show the dynamic response of the proposed grid power controller due to sudden cloud appearance (input disturbance), a typical scenario is illustrated in Fig.10. The figure shows abrupt changes of the PV power for 5 minutes due to sudden cloudy weather. The figure also shows the grid power, reference grid power and load variation during this period. The result shows that the measured grid power is following the reference grid power smoothly despite the variations of PV for a short period of time. Thus, show the robustness of the controller.

2) Case II: Effect of Abrupt Load Change: Load variation has influential effect on the dynamic performance of the system. In case II, an abrupt load variation has considered for a short period of time to observe the effect of load variation on controller performance. During this period, the output power from PV panel is kept almost constant. To show the dynamic response of the proposed grid power controller due to abrupt load change (output disturbance), a typical scenario is illustrated in Fig.11. In this scenario, the load power is suddenly dropped for 5 minutes due to abrupt load change for short duration. The dynamic performance of the controller on the event of abrupt load change illustrates in the figure. The result shows that the measured grid power is following the reference power with small fluctuations.

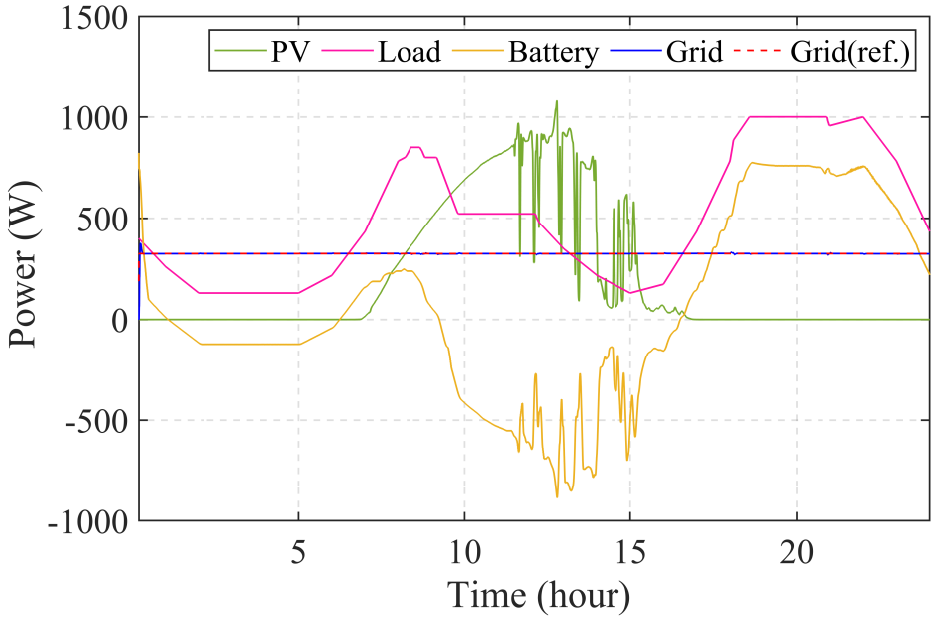

Fig. 15. PV generation, Residential load, battery power and grid power for typical winter days

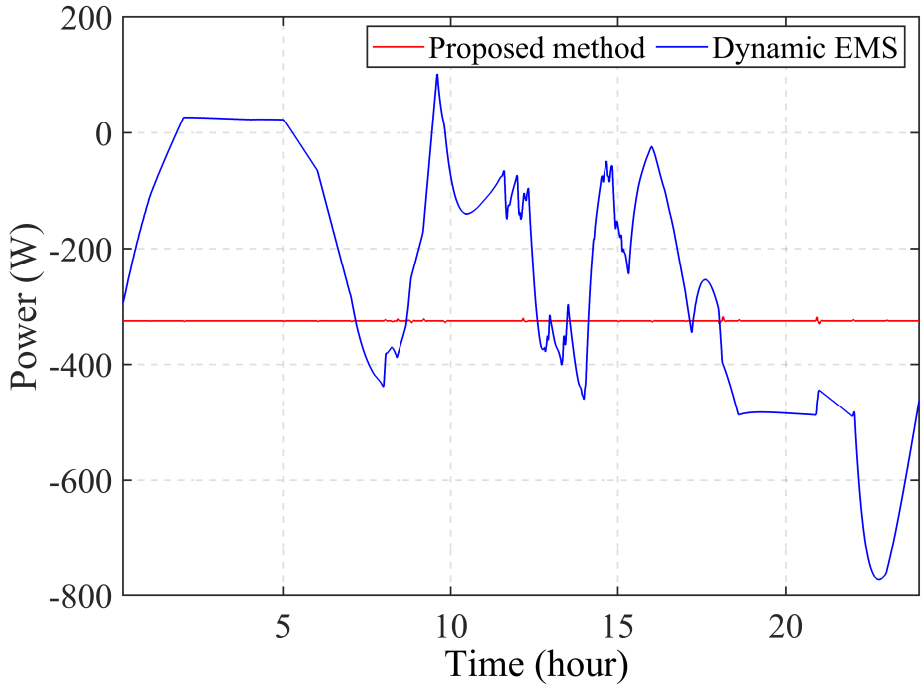

Fig. 16. Comparison of grid power for typical winter days

3) Case III: Controller Performance for a Typical Summer Day: For evaluating the controller performance for 24 hour duration using summer weather, a typical summer day (25th January 2017) weather information are chosen as an input of the PV panel. The sun radiation and temperature for a typical summer day are illustrated in Fig.12 that are used to generate the PV power for a typical summer day. A In addition, a residential load profile illustrated in Fig.13 is chosen to represent the load dynamics for a typical summer day. Apart from, Fig.13 also shows the battery power and grid power for typical summer days that follow the power balance equation of the MG. The results show that the proposed grid power control method is obtained a constant tie-line for a typical summer day despite the variation of PV and load power. However, the battery power fluctuation has increased significantly to obtain the objective.

4) Case IV:Controller Performance for a Typical Winter Day: To verify the performance of the controller for 24 hours on winter days weather and load variations, a typical winter day (4th June 2017) with the variation in temperature and radiation are chosen to generate the PV output in winter weather condition. The sun radiation and temperature for a typical winter day are shown in Fig.14. Moreover, the PV generation and residential load profile for a typical winter days are shown in Fig.15.

Besides that, Fig.15 also shows the battery power and grid power for a typical winter day. The result shows that grid power is following the reference for the simulation time and the power balance of the MG has obtained by required charging/discharging of the battery. The results proof that the MG has drawn a constant power from the grid to obtain a constant tie-line power on a typical winter day of the year.

B. Comparison

A comparison of grid power of the proposed inverter control method and dynamic EMS based control method [23] is presented in MATLAB to compare the performance between two control methods. In previous work [23], a fuzzy logic-based dynamic EMS is designed to control the buck-boost current controller of the battery storage to reduce the tie-line power fluctuation in a residential MG. Fig.16 shows the comparison of the grid power by using two different methods for a typical winter day. The result shows that the proposed inverter control has achieved a constant grid power for a typical day, whereas the dynamic EMS based method is showing many fluctuations. In other words, the proposed controller has achieved a robust control to obtain smooth tie-line compared with the dynamic EMS based control method.

V. Conclusion

In this paper, the concept of constant tie-line power method is proposed to overcome the tie-line power fluctuations in a grid-connected residential MG due to RESs and load variations. A grid current controller combined with a droop power controller is designed to keep a constant grid power drawn by the MG. The grid power reference is determined in the design stage based on the system dynamics. The power flow inside the MG is balanced through controlled charging/discharging of the battery. In addition, a state-space model of the MG system is derived for stability analysis of the system with the variation of system parameters. Furthermore, a simulation model is developed using the state-space model of the MG to verify the performance of the controller in different case studies. Moreover, a comparison with the previously addressed dynamic EMS approach is illustrated in simulation. The results show that with the application of the proposed control method, constant tie-line power can be obtained despite the short-term system fluctuations as well as for typical days of the year by maintaining the battery charging/discharging within a limit.

VI. List of Symbols and Abbreviations

List of Symbols

P_{pv}	PV power.
P_{load}	Load power.
P_g	Active grid power.
Q_g	Reactive grid power.
SoC	State of charge of battery.
SoC_{max}	Maximum value of SoC.
SoC_{min}	Minimum value of SoC.
d_2	Duty cycle of buck-boost converter.
d_1	Duty cycle of boost converter.
d_{dq}	Duty cycle of interlink inverter.
V_{dc}	DC link voltage.
V_{dc}^*	DC link reference voltage.
K_{p1}	Proportional gain of DC link voltage controller.
K_{i1}	Integral gain of DC link voltage controller.
K_{p2}	Proportional gain of grid current controller.
K_{i2}	Integral gain of grid current controller.
ω	Rated frequency.
m, n	Droop coefficient.
i_{gdq}	dq component of grid current.
i_{fdq}	dq component of filter current.
v_{idq}	dq component of inverter output voltage.
v_{odq}	dq component of filter capacitance voltage.
v_{gdq}	dq component of grid voltage.
L_f	Filter inductance.
L_g	Grid inductance.
C_f	Filter capacitance.
L_1	Inductance of boost converter.
L_2	Inductance of buck-boost converter.

C_{dc}	DC link capacitance.
i_1	PV current.
i_2	battery current.
R_f	Filter resistance.
R_g	Grid resistance.
R_1	Resistance of boost converter.
R_2	Resistance of buck-boost converter.
v_{pv}	Terminal voltage of PV.
v_{bat}	Terminal voltage of battery.
ω_{cPLL}	Cut-off frequency of PLL filter.
$K_{p,PLL}$	Proportional gain of PLL.
A, B, C, D	System coefficient of state-space equation.
x	State variables.
u	System inputs.
y	System outputs.

List of Abbreviations

DG	Distributed generation.
ESS	Energy storage system.
EMS	Energy management system.
MG	Microgrid.
$MPPT$	Maximum power point tracking.
$MGCC$	Microgrid controller.
PCC	Point of common coupling.
PLL	Phase locked loop.
$RESs$	Renewable energy resources.
SoC	State of charge.

REFERENCES

[1] E. Unamuno and J. A. Barrena, "Hybrid ac/dc microgrids—part i: Review and classification of topologies," *Renewable and Sustainable Energy Reviews*, vol. 52, pp. 1251–1259, 2015.

[2] J. P. Lopes, C. Moreira, and A. Madureira, "Defining control strategies for microgrids islanded operation," *IEEE Transactions on power systems*, vol. 21, no. 2, pp. 916–924, 2006.

[3] H. Bevrani and S. Shokoohi, "An intelligent droop control for simultaneous voltage and frequency regulation in islanded microgrids," *IEEE transactions on smart grid*, vol. 4, no. 3, pp. 1505–1513, 2013.

[4] C. Dou, X. An, D. Yue, and F. Li, "Two-level decentralized optimization power dispatch control strategies for an islanded microgrid without communication network," *International Transactions on Electrical Energy Systems*, vol. 27, no. 1, p. e2244, 2017.

[5] M. Hosseinzadeh and F. R. Salmasi, "Robust optimal power management system for a hybrid ac/dc micro-grid," *IEEE Transactions on Sustainable Energy*, vol. 6, no. 3, pp. 675–687, 2015.

[6] Y. Karimi, H. Oraee, M. S. Golsorkhi, and J. M. Guerrero, "Decentralized method for load sharing and power management in a pv/battery hybrid source islanded microgrid," *IEEE Transactions on Power Electronics*, vol. 32, no. 5, pp. 3525–3535, 2016.

[7] C. Zhang, W. Lin, D. Ke, and Y. Sun, "Smoothing tie-line power fluctuations for industrial microgrids by demand side control: An output regulation approach," *IEEE Transactions on Power Systems*, 2019.

[8] J. Shen, C. Jiang, Y. Liu, and J. Qian, "A microgrid energy management system with demand response for providing grid peak shaving," *Electric Power Components and Systems*, vol. 44, no. 8, pp. 843–852, 2016.

[9] Y. Sun, X. Tang, X. Sun, D. Jia, and G. Zhang, "Microgrid tie-line power fluctuation mitigation with virtual energy storage," *The Journal of Engineering*, vol. 2019, no. 16, pp. 1001–1004, 2019.

[10] D. Wang, S. Ge, H. Jia, C. Wang, Y. Zhou, N. Lu, and X. Kong, "A demand response and battery storage coordination algorithm for providing microgrid tie-line smoothing services," *IEEE Transactions on Sustainable Energy*, vol. 5, no. 2, pp. 476–486, 2014.

[11] J. Pascual, P. Sanchis, and L. Marroyo, "Implementation and control of a residential electrothermal microgrid based on renewable energies, a hybrid storage system and demand side management," *Energies*, vol. 7, no. 1, pp. 210–237, 2014.

[12] Y. Zhang, T. Zhang, R. Wang, Y. Liu, and B. Guo, "Optimal operation of a smart residential microgrid based on model predictive control by considering uncertainties and storage impacts," *Solar Energy*, vol. 122, pp. 1052–1065, 2015.

[13] J. Shen, C. Jiang, Y. Liu, X. Wang, and J. Qian, "Microgrid operation optimization with regulation of grid tie-line power fluctuations and risk management," *International Transactions on Electrical Energy Systems*, vol. 26, no. 11, pp. 2308–2321, 2016.

[14] S. Koohi-Kamali, N. Rahim, and H. Mokhlis, "Smart power management algorithm in microgrid consisting of photovoltaic, diesel, and battery storage plants considering variations in sunlight, temperature, and load," *Energy Conversion and Management*, vol. 84, pp. 562–582, 2014.

[15] M. BiazarGhadikolaei, M. Shahabi, and T. Barforoushi, "Expansion planning of energy storages in microgrid under uncertainties and demand response," *International Transactions on Electrical Energy Systems*, vol. 29, no. 11, p. e12110, 2019.

[16] J. Kathiresan, S. K. Natarajan, and G. Jothimani, "Energy management of distributed renewable energy sources for residential dc microgrid applications," *International Transactions on Electrical Energy Systems*, p. e12258, 2019.

[17] P. Malysz, S. Sirouspour, and A. Emadi, "An optimal energy storage control strategy for grid-connected microgrids," *IEEE Transactions on Smart Grid*, vol. 5, no. 4, pp. 1785–1796, 2014.

[18] A. C. Luna, N. L. Diaz, M. Graells, J. C. Vasquez, and J. M. Guerrero, "Mixed-integer-linear-programming-based energy management system for hybrid pv-wind-battery microgrids: Modeling, design, and experimental verification," *IEEE Transactions on Power Electronics*, vol. 32, no. 4, pp. 2769–2783, 2016.

[19] J. Pascual, J. Barricarte, P. Sanchis, and L. Marroyo, "Energy management strategy for a renewable-based residential microgrid with generation and demand forecasting," *Applied Energy*, vol. 158, pp. 12–25, 2015.
[20] D. Arcos-Aviles, J. Pascual, F. Guinjoan, L. Marroyo, P. Sanchis, and M. P. Marietta, "Low complexity energy management strategy for grid profile smoothing of a residential grid-connected microgrid using generation and demand forecasting," *Applied Energy*, vol. 205, pp. 69–84, 2017.
[21] D. Arcos-Aviles, J. Pascual, L. Marroyo, P. Sanchis, and F. Guinjoan, "Fuzzy logic-based energy management system design for residential grid-connected microgrids," *IEEE Transactions on Smart Grid*, 2016.
[22] Z.-x. Xiao, J. M. Guerrero, J. Shuang, D. Sera, E. Schaltz, and J. C. Vásquez, "Flat tie-line power scheduling control of grid-connected hybrid microgrids," *Applied energy*, vol. 210, pp. 786–799, 2018.
[23] M. Islam, F. Yang, C. Ekanayek, and M. Amin, "Grid power fluctuation reduction by fuzzy control based energy management system in residential microgrids," *International Transactions on Electrical Energy Systems*, p. e2758.
[24] M. A. Eltawil and Z. Zhao, "Mppt techniques for photovoltaic applications," *Renewable and sustainable energy reviews*, vol. 25, pp. 793–813, 2013.
[25] J. Schonbergerschonberger, R. Duke, and S. D. Round, "Dc-bus signaling: A distributed control strategy for a hybrid renewable nanogrid," *IEEE Transactions on Industrial Electronics*, vol. 53, no. 5, pp. 1453–1460, 2006.
[26] M. Rasheduzzaman, "Small signal modeling and analysis of microgrid systems," 2015.